On the Morphological Behavior of ABC Miktoarm Stars Containing Poly(cis 1,4-isoprene), Poly(styrene), and Poly(2-vinylpyridine)

Sergey Chernyy,[1] Jyoti P. Mahalik,[2,3] Rajeev Kumar,[2,3] Jacob Judas Kain Kirkensgaard,[4] Matthias M. L. Arras,[5] Hyeyoung Kim,[6] Lars Schulte,[1] Sokol Ndoni,[1] Gregory S. Smith,[5] Kell Mortensen,[4] Bobby G. Sumpter,[2,3] Thomas P. Russell,[6] Kristoffer Almdal[1]

[1]Technical University of Denmark, DTU Nanotech, Produktionstorvet, 2800 Lyngby, Denmark
[2]Center for Nanophase Materials Sciences, Oak Ridge National Laboratory, Oak Ridge, Tennessee 37831
[3]Computational Sciences and Engineering Division, Oak Ridge National Laboratory, Oak Ridge, Tennessee 37831
[4]Niels Bohr Institute, University of Copenhagen, 2100 Copenhagen, Denmark
[5]Neutron Scattering Division, Oak Ridge National Laboratory, Oak Ridge, Tennessee 37831
[6]Polymer Science and Engineering Department, University of Massachusetts Amherst, 120 Governors Drive, Amherst, Massachusetts 01003
Correspondence to: S. Chernyy (E-mail: sergeychernyy@gmail.com); J. P. Mahalik (E-mail: jpmahalik@gmail.com)

Received 23 May 2018; accepted 10 August 2018
DOI: 10.1002/polb.24733

ABSTRACT: Fundamental understanding of microphase separation in ABC miktoarm copolymers is vital to access a plethora of nonconventional morphologies. Miktoarm stars based on poly(*cis* 1,4-isoprene) (I), poly(styrene) (S), and poly(2-vinylpyridine) (V) are model systems, which allow systematic studies of the effects of composition, chemical microstructure, and temperature on the thermodynamics of microphase separation. Eleven ISV-*x* (I:S:V = 1:1:*x*, *v*:*v*:*v*) miktoarm copolymers were synthesized by anionic polymerization affording well-defined copolymers with a variable V arm. Equilibrium bulk morphologies of all samples, as evidenced by small-angle X-ray scattering, transmission electron microscopy (TEM), and self-consistent field theory, showed a systematic transition from lamellae ($x \approx$ 0–0.2) to [8.8.4] tiling ($x \approx$ 0.6–0.9) to cylinders in undulating lamellae ($x \approx$ 2–4) and, finally, to hexagonally packed core–shell cylinders ($x \approx$ 5–8). Chemical microstructure of the I arm [poly(*cis* 1,4-isoprene)] versus poly(3,4-isoprene) is shown to play important role in affecting morphological behavior. To reconcile differences between ISV-*x* star morphologies reported in the literature and those reported herein, even for the same composition, effects of the microstructure of I arm on the Flory–Huggins parameter between I and V arms were taken into account in a qualitative manner. © 2018 Wiley Periodicals, Inc. J. Polym. Sci., Part B: Polym. Phys. **2018**

KEYWORDS: ABC miktoarm stars; bis(phenylethenyl)benzene (1,4-PEB); bulk morphology; phase transition; poly(2-vinylpyridine) (V); poly(isoprene) (I); poly(styrene) (S)

INTRODUCTION ABC miktoarm star terpolymers—macromolecules containing three chemically distinct polymeric chains connected at one junction point—have attracted much interest due to the exceptional packing of the microdomains, both, in the bulk and in thin films, into tessellated morphologies.[1–7] Depending on the composition and the strength of interactions between the blocks, ABC star terpolymers can form cylindrical microdomains replicating some of the 12 Archimedean tiling patterns and hyperbolic tilings on a gyroidal net, cylinders in lamella, lamellae in lamella, lamellae in cylinder, and lamellae in sphere patterns—packings which are quite different from the microdomain morphologies typically seen for AB and linear ABC block copolymers.[4,6–9] Mixtures of ABC and ABD stars were shown theoretically to form one of the most complex soft matter morphologies known to date.[10,11]

ABC miktoarms offer a large variety of structures but at the cost of complexity in synthesis, characterization, and modeling in comparison to their linear block copolymer counterparts. The first synthesis of ABC miktoarm was based on chlorosilane chemistry where methyltrichlorosilane (compound **1** in Scheme 1) was used as a linking agent for three different arms. The method resulted in the synthesis of ISB [poly(isoprene), poly(styrene), poly(butadiene)], ISM [poly(isoprene), poly(styrene), poly(methyl methacrylate)], and ISD [poly(isoprene), poly(styrene), poly(dimethylsiloxane)] stars.[12–15] An alternate strategy used difunctional linking agents, normally a derivative of diphenylethylene (DPE) containing a nonhomopolymerizable double bond and an alkyl or silyl halide moiety. For example, compound **2** (Scheme 1), 1-(bromomethyl)-4-(1-phenylvinyl) benzene, was shown to react preferably

Additional Supporting Information may be found in the online version of this article.

with living macroanions via the bromomethyl group forming DPE end-capped macromonomer which could further add the second arm and initiate the third arm of the star terpolymer. Compounds **2–4** (Scheme 1) were used for the syntheses of SBM [poly(styrene), poly(butadiene), poly(methyl methacrylate)], SBV [poly(styrene), poly(butadiene), poly(2-vinylpyridine)], and ISV [poly(isoprene), poly(styrene), poly(2-vinylpyridine)] miktoarm stars.[16–19] In the present study, we prepared ISV miktoarm star terpolymers using the symmetrical difunctional linking agent **5**, 1,4-bis(phenylethenyl)benzene (1,4-PEB) which was previously used for the synthesis of AA'A" star homopolymers having S arms of different molecular weights.[20]

Morphologies of the ISV miktoarm star terpolymers have been studied in numerous laboratories. These terpolymers have been synthesized and characterized since 2000 to understand the influence of the composition of the components on the morphology.[18,19] A complete triangular phase diagram was constructed for ISV by Yushu et al.[4] based on their numerous studies,[4,9,18,19,21–25] and, in general, a number of theoretical studies focused on different aspects of the microphase separation in ABC miktoarms.[3,26–32] By changing the length of one of the arms, typically V, while keeping the other two arms (I and S) fixed, represented as ISV-*x*, where *x* is the volume ratio of V over I, it has been shown that, as *x* increases from 0.2 to 0.4 to 0.7 to 1.2 to 1.9 to 3 and then to 10, the morphology transitions from spheres sandwiched by lamellae to a [12.6.4] tiling, a [6.6.6], a [8.8.4], a [12.6.4] tiling, an alternating lamellae (ALT. LAM) and, finally, to cylinders in lamellae, respectively.[4] Modeling attempts have been made to simulate these morphological transitions.[3,26,33] Assuming symmetric interactions between the three pairs, a detailed triangular phase diagram has been constructed based on the self-consistent field theory (SCFT) calculations.[33] By combining generic spectral method and real-space methods, about a dozen different ordered morphologies were reported. However, it was noted that there were discrepancies between the simulated and experimentally observed morphologies, which were attributed mainly to the asymmetric interactions between the three different pairs. In other studies,[3,26] two interaction parameters (χ_{IS} and χ_{SV}) are assumed to be equal but less than χ_{IV}, that is, $\chi_{IS} \approx \chi_{SV} < \chi_{IV}$. Using this simplified model, it was possible to mimic some ISV-*x* morphologies observed in the experiments. Here, we undertook the challenge to understand the effects of additional variables and go beyond the simplified model.

Most studies have focused on understanding the effects of composition without considering annealing temperature, molecular weight, and the specific chemistry of the systems. In fact, chemical structure of the constituent arms exerts a secondary effect on the morphology, as long as the balance of interaction parameters and volume ratios of the arms (*v*:*v*:*v*) remain unchanged. For example, ISF miktoarm stars [F represents poly(ferrocenylethylmethylsilane)] show morphologies identical to ISV systems: [12.6.4], [8.8.4], and ALT. LAM was found for both ISV and ISF systems having similar compositions of (1:1:0.4) vs. (1:0.9:0.6), (1:1:1.2) vs. (1:1.3:0.7), and (1:1:3) vs. (1,0.7:3.3), respectively, since the interaction parameters of ISF ($\chi_{IS} \approx \chi_{SF} < \chi_{IF}$) are similar, relative to those of ISV.[4,34] However, pairwise interactions can be affected by the microstructure of the I component in the ISV systems.[35] Specifically, we show that in virtually an identical chemical system the microstructure of the poly(isoprene), that is, *cis* 1,4 or 3,4 configuration, can alter the interactions sufficiently to generate different bulk morphologies. We qualitatively show that ISV stars containing poly(*cis* 1,4-isoprene) have more imbalanced interaction parameters ($\chi_{IS} \approx \chi_{SV} \ll \chi_{IV}$) in comparison to ISV containing poly(3,4-isoprene) [$\chi_{IS} \approx \chi_{SV} < \chi_{IV}$].

We investigated ISV miktoarm star terpolymers with fixed relative volumes of the I and S arms and varied the relative volume of the V arm (v_I: v_S: v_V; 1: 1: *x*; *x* = 0–7.6), covering essentially the entire height of the ternary phase diagram (SI1, Supporting Information). Systematically changing the composition by a direct synthesis, rather than by blending a homopolymer with an ISV arm precursor, allowed us to observe a gradual morphological change from LAM ($x \approx 0$–0.2) to [8.8.4] tiling ($x \approx 0.6$–0.9) to cylinders in undulating lamellae (CYLULAM) ($x \approx 2$–4), finally, to hexagonally packed core–shell cylinders ($x \approx 5$–8). This comprehensive set of experimental data on one miktoarm star terpolymer series lends itself to a comparison between experiment and theory on the morphological impact of temperature, chain length, and segmental interactions.

EXPERIMENTAL

All chemicals were purchased from Sigma-Aldrich unless otherwise stated. Tetrahydrofuran (THF) was distilled over a sodium-benzophenone mixture after it reached a violet color. Cyclohexane was distilled from living yellowish poly(styryl)-Li. Monomers, styrene, isoprene, and 2-vinylpyridine (2VP) were passed through basic aluminum oxide column, distilled from calcium hydride and then either from dibutylmagnesium (styrene and isoprene), or triethylaluminum (2VP) prior to use. *Sec*-butyllithium (*sec*-BuLi, 1.4 M in cyclohexane) was used as an initiator. The apparatus for anionic polymerization was described in details elsewhere.[36,37]

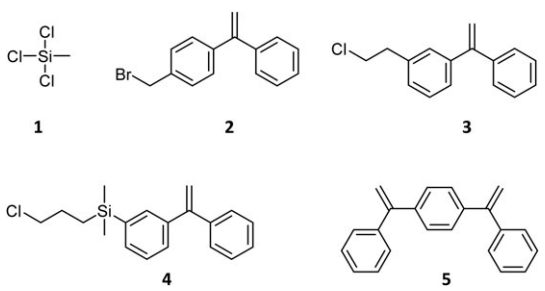

SCHEME 1 Various capping agents used for synthesis of the star shaped polymers.

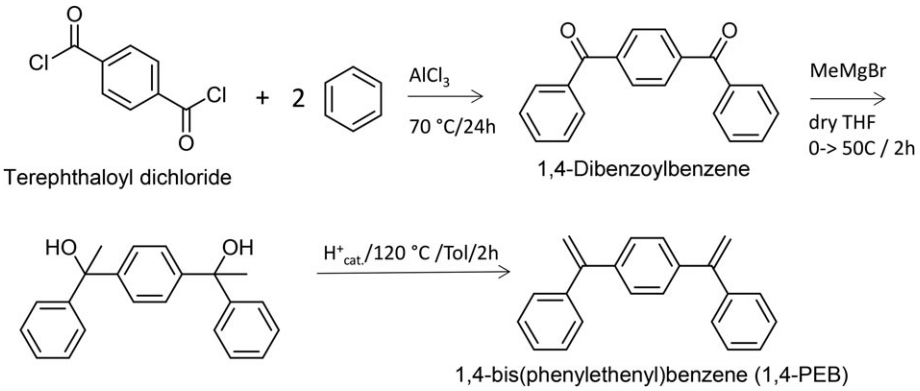

SCHEME 2 The synthesis procedure for preparation of the linking agent used in this work.

Synthesis of the Linking Agent (1,4-PEB)

Terephthaloyl dichloride (81.2 g, 0.400 mol) was dissolved in 500 ml dry benzene (Na-benzophenone) and slowly added to 117 g (0.877 mol) of $AlCl_3$ in 500 ml dry benzene. The mixture was heated to 60 °C for 0.5 h (HCl evolution) and then for 1 day at 70 °C. To the yellow slurry, 1 L of cold water and 25 ml of 37% HCl were added slowly followed by 0.5 L of chloroform. The organic phase was collected and the aqueous phase was extracted with 0.5 L of chloroform. The organic phases were combined, washed with 0.5 L of 2% $NaHCO_3$, then twice with water. The solvent was evaporated and a yellowish solid, 1,4-dibenzoylbenzene, was recrystallized from acetone/methanol mixture resulting in 87.5 g of white crystalline solid, with a yield of 77%. In a second step, 1,4-dibenzoylbenzene solution in THF (87.5 g, 0.306 mol) was added dropwise to a solution of methyl magnesium bromide in THF (0.696 mol) at 0 °C resulting in dark red solution. After 1 h, the mixture was heated to 50 °C for 1 h followed by quenching with 10 ml of water and 0.4 L of 2 M HCl. A procedure similar to the one described above yielded 95 g of yellowish tertiary alcohol oil [1,1′-(1,4-phenylene)bis(1-phenylethan-1-ol)]. In a the third step, 95 g of the tertiary alcohol was subjected to azeotropic dehydration by refluxing it in toluene with one tip of *p*-toluenesulfonic acid resulting in 58 g of 1,4-PEB. The final product was obtained with 51% yield relative to starting terephthaloyl dichloride after recrystallization from acetone/methanol in a form of colorless crystals (Scheme 2). ^{1}H NMR: ($CDCl_3$, 400 MHz): 5.55 ppm (dd, J = 17.8, 1.2 Hz, 4H), 7.57–7.28 ppm (m, 14H).

Synthesis of ISV Stars

First, a polymerization of isoprene was carried out in cyclohexane at 40 °C for 10 h using *sec*-BuLi as an initiator affording poly(isoprene) consisting mostly of 1,4 monomer units (75% *cis* 1,4, 20% *trans* 1,4, and 5% 3,4 microstructure).[5] The solution of living poly(isoprenyl)-Li was transferred to the second reactor containing two times excess of the 1,4-PEB in THF at −15 °C. The coupling reaction was performed at −15 °C for 8 h, followed by quenching in methanol with a repetitive precipitation of the resulting macromonomer from THF to methanol. The second arm was added by titrating the macromonomer solution in THF with the solution of living poly(styryl)-Li at −78 °C. Subsequently, a predetermined amount of 2VP was added to the reactor and a 150 ml aliquot was taken after 1 h at −78 °C prior to adding a new portion of 2VP. The process was repeated resulting in a formation of ISV stars with different molecular weights of the V component (Scheme 3, Table 1, and SI2, Supporting Information).

Characterization

The polydispersity (PDI) was determined by gel permeation chromatography (GPC) using THF with 1% of triethylamine as an eluent at 0.5 ml min^{-1} flow rate with a column set consisting of a precolumn and two 300 × 8 mm columns (PLgel Mixed C and Mixed D). The stationary phase was crosslinked poly(styrene-divinylbenzene). The system was equipped with triple detection: a combined Viscotek model 200 differential refractive index detector, a differential viscosity detector, and a Viscotek model LD 600 right angle laser light scattering detector. Rheological characterization was performed on a Rheometrics solids analyzer operated with a 0.5 mm shear gap sandwich configuration at 1% shear strain (γ) amplitude and 1 rad s^{-1} frequency (ω). All rheological data were obtained on heating the specimens from a disordered state under nitrogen flow to avoid sample degradation.[38,39] For transmission electron microscopy (TEM) and small-angle X-ray scattering (SAXS) about 0.5 mm polymer films were produced by solvent casting from 7% THF solutions under nitrogen for 1 week in the dark followed by thermal annealing at 150, 175, or 200 °C for 5, 3, or 1 days, respectively, at ~0.001 mbar in the homebuilt vacuum chamber. Annealed samples were stained with 0.1 ml 4% OsO_4 aqueous solution for 16 h, microtomed at room temperature to a thickness of 70 nm, then further stained with I_2 for 2 h on copper grids, unless noted otherwise. The TEM was performed on FEI Tecnai T20 G^2 at 200 kV accelerating voltage in the bright field mode. SAXS profiles were measured using a SAXSLab instrument equipped with a Rigaku 40 W microfocused Cu-source (λ = 1.54 Å) and a moveable Pilatus 300 k pixel detector. Samples were mounted in small Cu-discs between two 5–7 μm mica windows prior to measurements.

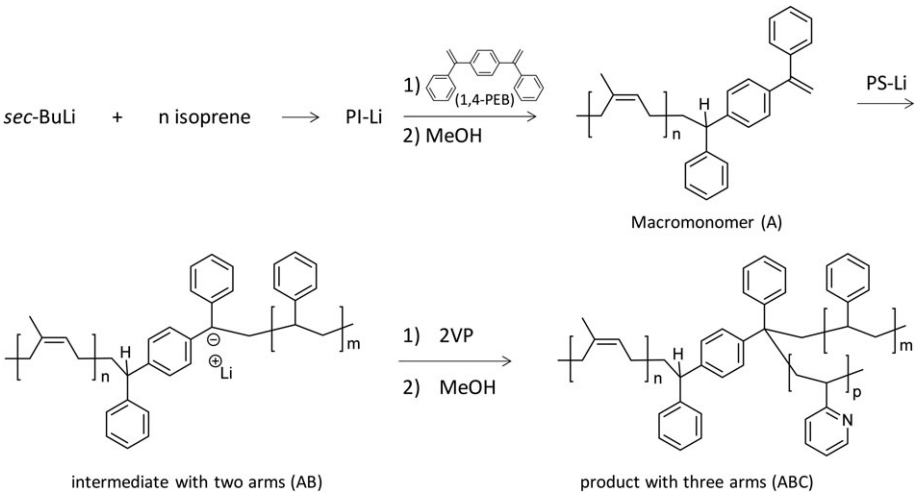

SCHEME 3 The procedure used for synthesis of ISV miktoarm star terpolymers.

Self-Consistent Field Theory

Equilibrium morphologies of the ISV-*x* samples were simulated using standard SCFT-based simulations. For obtaining the equilibrium morphologies, random as well as different cylindrical and lamellar kind of structures (ALT. LAM, CYLULAM structure, Lamellar-3 [LAM-3]) were used as initial conditions. The cylindrical structures used as initial conditions were: five tiling structures: [12.6.4], [6.6.6], [8.8.4], [8.6.6; 8.6.4], [10.6.6; 8.8.4], and core–shell hexagonally packed structure. The free energies of the resulting structures were compared to determine a morphology with the lowest free energy. ABC terpolymers have been studied extensively using the SCFT.[3,26,30,31,40,41] A brief description of the SCFT model and the parameters used for ISV-*x* is presented below. Following standard protocol[42] for the SCFT, a Hamiltonian of the ABC miktoarm melt was defined, followed by field theoretical transformations leading to a field theory. The saddle-point approximation was then applied to approximate functional integrals appearing in the field theory, which yield a set of nonlinear equations. These equations were then solved iteratively to obtain volume fraction distribution of the three different components (I, S, and V). Polyswift ++[45] was used for all the SCFT calculations in this article, which uses a pseudo-spectral method[43,44] for solving modified diffusion equations appearing at the saddle point. Briefly described below is the Hamiltonian of the ISV-*x* system.

A Gaussian chain model was used to represent the three arms of the miktoarm polymer, made up of N number of total segments, each segment having the same length $b = v^{1/3}$, where $v = (v_S v_I v_V)^{1/3}$ is the geometric mean of the molar volume of the polymer segments, v_S, v_I, and v_V being the molar monomer volume of S, I, and V, respectively. Conformational asymmetry was not considered in the model for computational efficiency as well as due to the fact that the parameters were not too different for the three components. The conformational asymmetry parameters ($\beta_i^2 = b_i^2/6v_i$)[46] in units of nm^{-1} for PS, PI, and P2VP are 0.305, 0.334, and 0.312, respectively, where $b_i = v_i^{1/3}$. The maximum ratio of the conformational asymmetry parameter for the SIV copolymers is 1.1 ($=\beta_{PI}^2/\beta_{PS}^2$). The conformational asymmetry effects are the most significant near disorder-sphere transition boundaries in block copolymers due to shift of the critical point and resulting skewing of the morphology diagrams.[47] Typically, one requires higher values of the conformational asymmetry parameter in order to see noticeable changes.[47] For example, in a recent work by Schulze et al.,[48] conformational asymmetry stabilizes the Frank–Kasper phase when the ratio of the asymmetry parameter is 1.32 and no significant changes were observed for a lower value (=1.06). In this work, we have investigated intermediate-strong segregation regimes for either lamellar, cylinder or tessellated morphologies with relatively small conformational asymmetry parameters (~1.1). For such systems far from the disorder–order transition boundaries, we expect the conformational asymmetry effects to be minimal,[47] which is also justified by *posteriori* qualitative agreements between experiments and SCFT results. As the conformational asymmetry effects in ABC miktoarm copolymers remain largely unexplored, a detailed study is required to explore possible effects in the context of SIV miktoarm polymers. With a choice of an average segment length for all the three components, the system can be scaled with respect to the radius of gyration of the complete chain ($R_g = b(N/6)^{1/2}$, where $N = \sum_{i=1}^{3} N_i$), whereas, if conformational asymmetry is considered, then the system needs to be scaled with respect to the radius of gyration corresponding to the block with smallest conformational asymmetry. The later choice entails larger number of grid points for simulating a unit cell. Each arm of the terpolymer was assumed to have $f_i N$ number of segments so that $f_i = N_i/N$, where N_i was defined as the ratio of the molar volume of the polymer to v and $N = \sum_{i=1}^{3} N_i = \frac{1}{v}\sum_{i=1}^{3} \frac{M_{ni}}{\rho_i}$. The densities ρ_i of S, I, and V were taken to be (in g ml^{-1}) 1.06, 0.91 and 1.15, respectively. The polymer molecular weights MN_i of I and S are presented in the first and second columns of Table 1, respectively. For V

TABLE 1 Characteristics of ISV Star Terpolymers and their Precursors

Name	[a]Mn (kDa)	[b]PDI	[c]IxSyVz volume ratios x:y:z	[d]Morphology	[d]*d*-spacing (nm)
I	9.8	1.05	1: 0: 0	homogenous	n/a
S	11.6	1.05	0: 1: 0	homogenous	n/a
IS	21.4	1.04	1: 1: 0	LAM	19.4
ISV-0.04	21.9	1.07	1: 1: 0.04	LAM-3	19.8
ISV-0.15	23.3	1.07	1: 1: 0.15	LAM-3	20.4
ISV-0.33	25.5	1.07	1: 1: 0.33	[12.6.4] and/or [8.6.6; 8.6.4]	21.2
ISV-0.62	29.1	1.07	1: 1: 0.62	[8.8.4]	22.3
ISV-0.9	32.5	1.09	1: 1: 0.9	[8.8.4]	23.1
ISV-1.9	44.6	1.11	1: 1: 1.9	CYLULAM	28.8
ISV-2.9	56.7	1.12	1: 1: 2.9	CYLULAM	34.5
ISV-4.0	70.7	1.14	1: 1: 4.0	CYLULAM	40.5
ISV-5.2	85.5	1.18	1: 1: 5.2	HEX	42.4
ISV-7.6	116	1.29	1: 1: 7.6	HEX	45.5

[a] Determined from GPC and NMR in $CDCl_3$.
[b] Determined from GPC.
[c] Volume ratios of I, S, and V blocks were calculated from NMR and polymer densities (ρ_{PI} = 0.91 g ml^{-1}, ρ_{PS} = 1.06 g ml^{-1}, ρ_{P2VP} = 1.15 g ml^{-1}).
[d] Lamellar (LAM), Lamellar-3 (LAM-3), [12.6.4] Archimedean tiling ([12.6.4]), [8.6.6; 8.6.4] Archimedean tiling ([8.6.6; 8.6.4]), [8.8.4] Archimedean tiling ([8.8.4]), cylinders in undulating lamellae (CYLULAM) structure and hexagonally packed core–shell cylinders (HEX) morphologies and *d*-spacing ($d = 2\pi/q^*$) were assessed by SAXS.

the molecular weight is obtained by subtracting the IS molecular weight (third column of Table 1) from any given ISV-x sample molecular weight. For all the SCFT calculations, the length scales were scaled with respect to $R_g = b(N/6)^{1/2}$. The interaction parameters were obtained from reports in the literature: χ_{IS} and χ_{SV} are reported to be 0.0737[49] and 0.0895[50] at 175 °C—the annealing temperature for most of the samples. Some samples had an annealing temperature of 150 °C, but due to the lack of a quantitative temperature dependence of the interaction parameter for PI-P2VP, 175 °C was kept constant for all the samples in the SCFT calculations unlike the experimental conditions. Moreover, our studies on the ISV-*x* samples revealed that the temperature has hardly any effect on the morphology of the polymers except for one of the samples. The χ_{IV} is reported to be about eight times of χ_{IS} based on solubility parameter estimations.[51] For computational purposes, $\chi_{IV} = K\chi_{IS}$ was chosen, where K was varied to obtain the morphologies observed using SAXS and TEM in this work and a value of 3.5 was found to suitably represent most of the observed morphologies. The calculations were done in two-dimensional (2D) for all the cases and in three dimensional (3D) for those samples for which experimental data were available. For the 2D calculations, the initial conditions for the fields and the box dimensions ($L_x/R_g = L_y/R_g$) were varied between 7.0 and 13.5 to obtain the morphologies with minimum free energies. The grid size was varied between 0.08 R_g and 0.21 R_g for either 64 × 64 or 96 × 96 lattice. The free energies of the competing structures were presented in the Supporting Information (section SI9) (systems without competing ordered structures are not shown). For most of the cases, the free energy differences were significant enough to determine the equilibrium morphology.

3D calculations were also done for some samples. The objective behind the 3D calculations was to ascertain that the structures observed under TEM and SAXS are indeed 2D structures and the structures repeat in the third dimension. For the samples with $x < 1$ (ISV-0.04, ISV-0.15, ISV-0.33, ISV-0.62, and ISV-0.90), the symmetry observed in the free energy minima structure were obtained directly from a disordered state. Those structures were then subjected to zone annealing,[46] which resulted in no changes in the symmetries. For the samples with $x > 1$ (ISV-1.9, ISV-2.9, ISV-4, ISV-5.2, and ISV-7.6) χN values were gradually increased to obtain the final morphologies from disordered state. These final structures were then subjected to zone annealing which again resulted in no changes in the symmetries. Field relaxation parameter $\geq$0.05 were chosen for lower χN values.[44] The simulation box parameters for ISV-0.04 were: 32 × 32 × 32 lattice grid with $0.16R_g$ spacing, for ISV-0.15, ISV-0.33, ISV-0.62, and ISV-0.9: 64 × 64 × 16 with grid size varying between $0.1R_g$ and $0.16R_g$, for ISV-1.9, ISV-2.9, ISV-4.0, ISV-5.2, and ISV-7.6: 96 × 96 × 16 grids with grid size varying from 0.09 R_g to 0.15 R_g. A summary of the various parameters used in these calculations is given in Table S1, Supporting Information.

Static Structure Factor from Volume Fraction Distributions

Scattering patterns were calculated from the volume fraction distributions obtained using the SCFT. The volumetric mean of the scattering length density (SLD) at every grid point was assumed to represent the spatial distribution of the SLD, that is, $\rho(x,y) = \sum_{i=1}^{3} \mathrm{SLD}_i \phi_i(x,y)$, where the subscript i represents I, S, and V and ϕ_i represents the volume fraction of the respective component. The SLDs of I, S, and V were taken to be 8.7, 9.5, and 10.3 × 10^{-6} Å^{-2}, respectively. The FFTW library[52] was used for the Fourier transformation of ρ(x,y) (Θ(q_x,q_y) = Fourier transform {ρ(x,y)}), where $q_x = 2\pi m/L_x$, and $q_y = 2\pi n/L_y$ are the scattering wave vector components

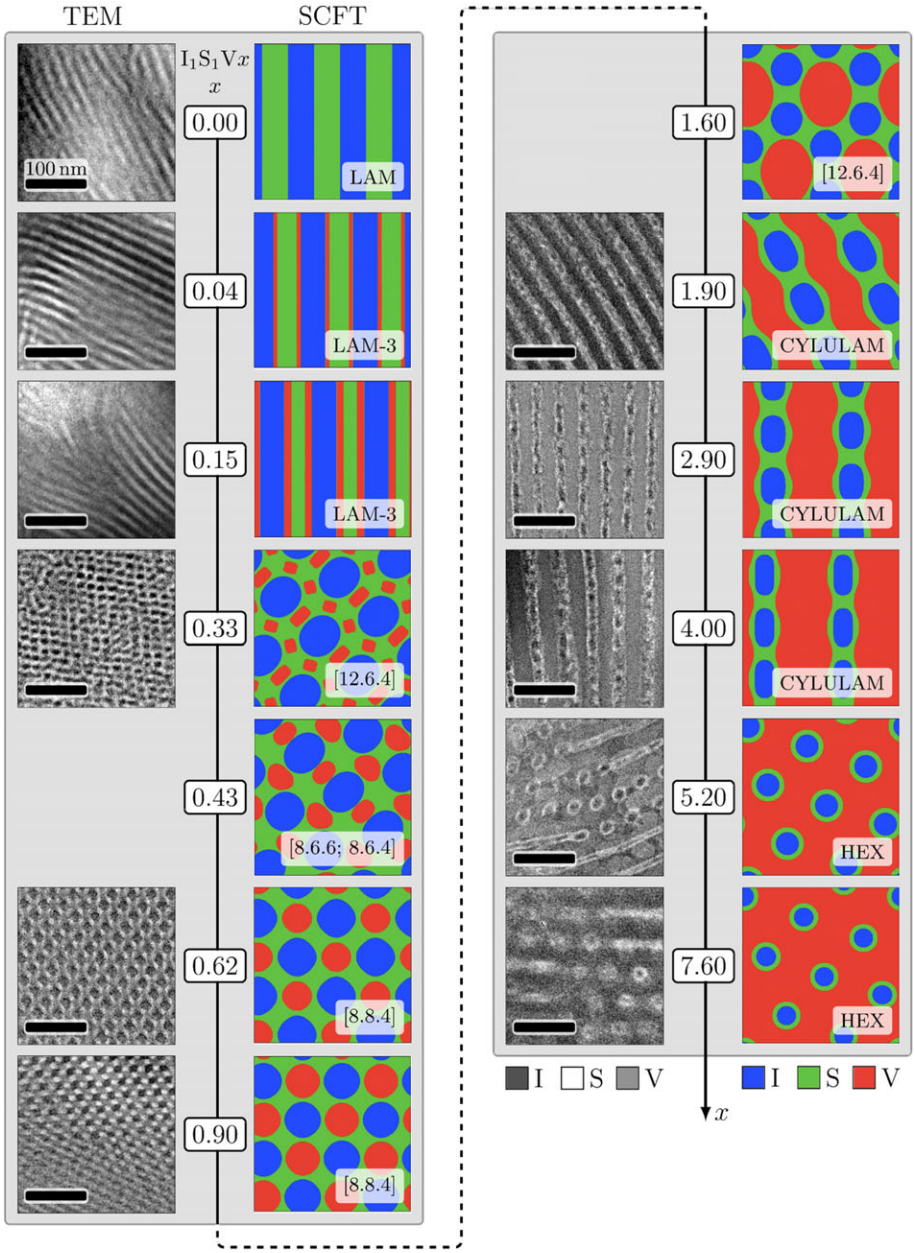

FIGURE 1 Morphology of ISV-x (1:1:x) as a function of the volume fraction $x = v_V/v_I$, whose values are shown along the line. The images shown to the left of the line are obtained using TEM and those to the right are obtained using the SCFT. For the TEM images, the samples were annealed at 150 °C for $0 \le x \le 0.62$ and 175 °C for the rest. All samples, except for IS which was stained with OsO_4, were consecutively stained with OsO_4 and I_2. The black, white, and gray colors correspond to I, S, and V domains, where applicable. The scale bar is 100 nm in all the cases. The SCFT yields the volume fraction of the three components (as shown in Fig. 2) and the component with maximum volume fraction at any grid point is used to color that point, except for the samples $0.04 \le x \le 0.33$ due to the miscibility of V in S at such low volume fraction. For these three cases, maximum volume fraction of either I or S, or, if the volume fraction of V exceeds a certain cut-off value (cut-off value is set to 0.048, 0.1055, and 0.25 for ISV-0.04, ISV-0.15, and ISV-0.33, respectively) is used to color each grid point. Color code for the SCFT images, blue: I, green: S, and red: V. The morphology transitions from LAM (IS) to LAM-3 (ISV-0.04 and ISV-0.15) to different tiling structures ([12.6.4] for ISV-0.33, [8.6.6; 8.6.4] for ISV-0.43, [8.8.4] for ISV-0.62 and ISV-0.9 and [12.6.4] for ISV-1.6) to CYLULAM (ISV-1.9, ISV-2.9, and ISV-4) and finally to core–shell hexagonal microstructure (ISV-5.2 and ISV-7.6) as x is gradually increased from 0 to 7.6. [Color figure can be viewed at wileyonlinelibrary.com]

in the x, and y directions, respectively, L_x and L_y represent the total length of the grids in the x and y directions, respectively. m and n are the integers ranging from 0 to $N_x/2$ and 0 to $N_y/2$, respectively, so that N_x and N_y are the number of grid points in x and y directions, respectively. The static structure factor S(q*) was obtained as a function

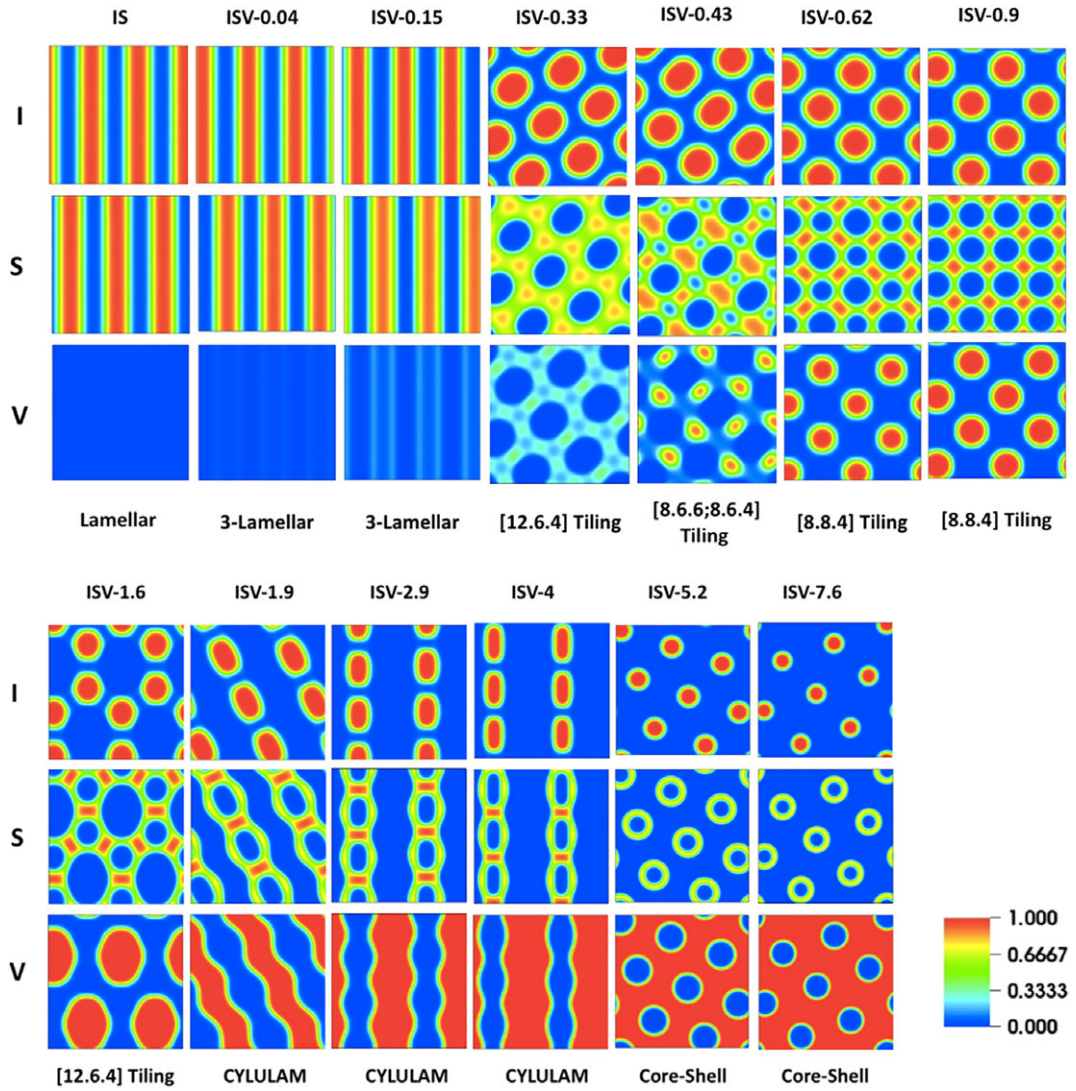

FIGURE 2 Detailed SCFT equilibrium volume fraction distribution of I, S, and V as a function of *x*, where *x* is the volume ratio of V over I (volume of I and S are kept fixed for all the samples and they are equal to each other). Here, *x* is varied between 0 and 7.6. Starting with lamellar profile for IS, the morphology evolved into 3-Lamellar (3-LAM) (ISV-0.04 and ISV-0.15), [12.6.4] tiling (ISV-0.33), [8.6.6; 8.6.4] tiling (ISV-0.43), [8.8.4] tiling (ISV-0.62 and ISV-0.9), [12.6.4] tiling (ISV-1.6), CYLULAM (ISV-1.9, ISV-2.9, and ISV-4), and finally to core–shell structure (ISV-5.2 and ISV-7.6) as the volume ratio of V over I is gradually increased from 0 to 7.6. For ISV-0.04 to ISV-0.33, V is miscible in S but for the other samples, it segregates into its own distinct domain. The color bar for volume fraction at the bottom right is shown for reference. The volume fraction of the three different components are not binary (the volume fraction is not zero or unity at any grid) as one would get an impression from SCFT images presented in Figure 1, the interfaces between the different components are smooth. [Color figure can be viewed at wileyonlinelibrary.com]

of the scalar wavevector $q^*(=(q_x^2 + q_y^2)^{1/2})$ using its definition: $S(q^*) = \langle\Theta(\mathbf{q}^*)\Theta(-\mathbf{q}^*)\rangle/(N_xN_y)$, so that $\Theta(\mathbf{q}^*)$ and $\Theta(-\mathbf{q}^*)$ represent the Fourier transform of ρ(x,y) and it's complex conjugate, respectively, at the Fourier wavevector $\mathbf{q}^*$. The angular bracket <> represented azimuthally averaged value of $S(q^*)$ at any given q^*.

RESULTS AND DISCUSSION

Eleven different samples of ABC miktoarm star terpolymers (Table 1 and SI2, Supporting Information) were prepared consisting of poly(*cis* 1,4-isoprene) (I), poly(styrene) (S), and poly(2-vinylpyridine) (V) arms by keeping the volume ratio $v_S/v_I = 1$ for all the samples while varying the volume ratio v_V/v_I between 0 and 7.6. The volume ratio $x = v_V/v_I$ was used to denote the samples as ISV-*x*, short for ISV (1:1:*x*, *v*:*v*:*v*). The results of the experimental characterizations and computational modeling are presented and discussed in the following.

The symmetric diblock copolymer IS showed the expected LAM morphology (Figs. 1 and 2) below the order-to-disorder

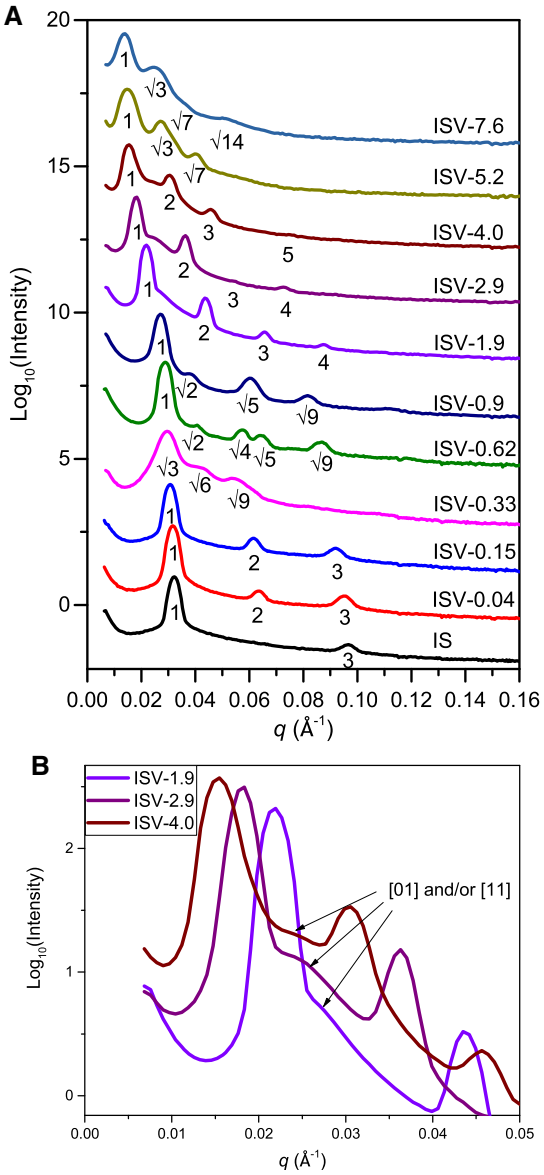

FIGURE 3 (A) SAXS results for ISV-x samples; annealing temperature is 150 °C for $0 \le x \le 0.33$, 200 °C for $x = 0.62$ and 175 °C for the rest. The scattering peaks are consistent with the real space morphologies obtained using TEM. (B) Zoom in of the [01] and/or [11] peak for the samples: ISV-1.9, ISV-2.9, and ISV-4. [Color figure can be viewed at wileyonlinelibrary.com]

transition (ODT) temperature (T_{ODT}) from TEM images and the SCFT calculations. Attachment of a small arm of V (ISV-0.04 and ISV-0.15) does not change the LAM morphology, as seen in the TEM images (Fig. 1), in fact, it is difficult to locate the V domain in the TEM images, since the volume fraction of V is small. However, the SCFT calculations show that the V is located at the interface between I and S so as to reduce the number of contacts between I and S domains (Fig. 2). Based on the $N\chi$ values reported in Table S1, Supporting Information, V is expected to be more miscible in S than in I. The SAXS results (Fig. 3) and computed scattering patterns based on the SCFT using the volume averaged electron SLD of the components (Fig. 4) also show the expected peaks for a LAM structure with

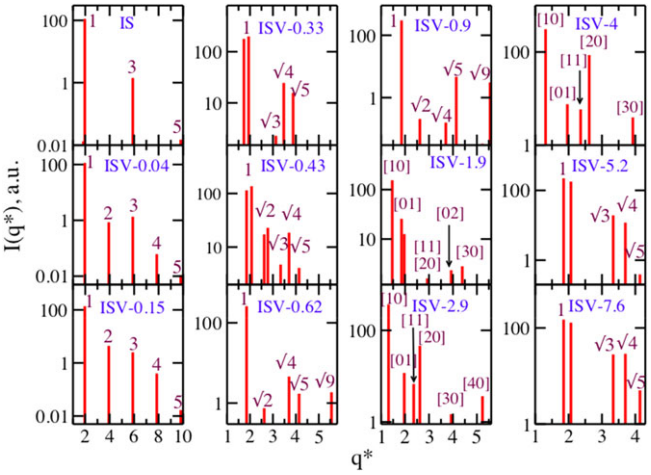

FIGURE 4 Scattering patterns predicted by the SCFT based simulations and obtained by Fourier transformation of the volume averaged electron SLD at all the grid points (electron SLD of I, S and V are (x 10^{-6} Å^{-2}) 8.7, 9.5, and 10.3, respectively). The equilibrium volume fraction distributions were obtained using the SCFT. The calculated scattering patterns qualitatively agree with that obtained using SAXS except for ISV-0.33. For the cases of ISV-1.9, ISV-2.9, and ISV-4, there are two different length scales in these hierarchical structure. Details of the analysis are presented in section SI4, Supporting Information. [Color figure can be viewed at wileyonlinelibrary.com]

q/q* values of 1:2:3.[5] For IS, only the odd reflections were observed (1:3:5) because of the perfect symmetry in composition. This symmetry was, however, broken when only a small amount of V was added and the even order reflections for the LAM structure reappear for ISV-0.04 and ISV-0.15. This is in agreement with the SCFT prediction that V segregates selectively to the S side of the LAM interface and is more miscible in S than in I.

Further increasing the V arm length (ISV-0.33) should lead to the [12.6.4] Archimedean tiling structure according to the SCFT calculations. The TEM images appear to qualitatively agree with the SCFT results with the V component having diminishing contrast, due to preferential miscibility with the S phase. Quantitatively, for ISV-0.33, SAXS peaks (cf. Fig. 3) are indexed at q/q* as 1:√2:√3.33, which could also be rewritten as integer Miller indices √3:√6:√9, whereas the SCFT calculations yield peaks at q/q* of 1:√3:√4:√5 for the [12.6.4] tiling (cf. Fig. 4). The SAXS peaks (√3:√6:√9) would imply cubic system with (111) as the first reflection, (112) the second, and (300) the third, whereas the SCFT results are consistent with that for the [12.6.4] structure reported in the literature.[3] However, the SCFT calculations for a slightly longer V arm (ISV-0.43) yielded [8.6.6; 8.6.4] tiling structures (Figs. 1 and 2) with corresponding scattering peaks located at q/q* of 1:√2:√3:√4:√5 (Fig. 4). Experimentally, it is challenging to ascertain whether [12.6.4] or [8.6.6; 8.6.4] tiling morphology is observed for ISV-0.33, especially, considering that SAXS peaks are very broad compared to those of the other samples, indicating less order or perhaps coexisting phases. The discrepancy between experiment and theory may arise from: (a) the SCFT parameters not being

TABLE 2 Comparison of the Morphologies found in the Current Studies with the Literature Reported Morphologies for ISV-*x* Miktoarms of Similar Composition

Source	Composition (volume ratio I/I:S/I:V/I)	Total MW (kDa)	Annealing temperature (°C)	Microstructure of poly(isoprene)	Morphology
Current	1:1:0.33	25.5	150	75% *cis* 1,4, 20% *trans* 1,4, 5% 3,4;	[12.6.4]
Literature[4]	1:1:0.4	10.8	150	74% 3,4; 26% 1,2	[12.6.4]
Current	1:1:0.62	29.1	150/200	75% *cis* 1,4, 20% *trans* 1,4, 5% 3,4;	[8.8.4]
Literature[4]	1:1:0.7	12.7	150	74% 3,4; 26% 1,2	[6.6.6]
Literature[19,23]	1:1.08:0.71	13.4	140	74% 3,4; 26% 1,2	[6.6.6]
Current	1:1:0.9	32.5	150/175/250	75% *cis* 1,4, 20% *trans* 1,4, 5% 3,4;	[8.8.4]
Current	1:1:1.9	44.6	175	75% *cis* 1,4, 20% *trans* 1,4, 5% 3,4;	CYLULAM
Literature[4,19,23]	1:1:1.9	18.8–19.9	140/150	74% 3,4; 26% 1,2	[12.6.4]
Current	1:1:2.9	56.7	175	75% *cis* 1,4, 20% *trans* 1,4, 5% 3,4;	CYLULAM
Literature[4]	1:1:3.0	23.9	150	74% 3,4; 26% 1,2	ALT. LAM

exactly the same as in experiment, (b) the PDI[53] of the synthesized copolymers which may impact the morphology leading to [8.6.6; 8.6.4] tiling, and/or (c) the coexistence of two different phases ([12.6.4] and [8.6.6; 8.6.4]) in the experiment.

Further increasing the length of V (ISV-0.62 and ISV-0.9), leads to a [8.8.4] tiling structure. The ISV-0.62 attains a well-ordered morphology upon heat annealing to 150 °C (Fig. 1). All three components, characterized by black (I), gray (V), and white (S), are distinguishable in ISV-0.62, indicating a high degree of microphase separation. The volume fraction distribution (Fig. 2) also indicates that V is highly segregated for this composition in comparison to the other systems with lower V contents (ISV-0.04, ISV-0.15, and ISV-0.33). The TEM images and the SCFT calculations show that a square lattice is formed and the S domains (white in the TEM image and green in the SCFT calculations) have four nearest neighbors (two distinct domains of V and two distinct domains of I) whereas both V and I have eight nearest neighbors: four distinct domains of S and four distinct domains of I (for V) or V (for I). The SAXS and the SCFT-based scattering patterns qualitatively agree, showing peaks at q/q* of 1:$\sqrt{2}$:$\sqrt{4}$:$\sqrt{5}$:$\sqrt{9}$ (for ISV-0.9 SAXS, $\sqrt{4}$ peak is absent). These peaks qualitatively agree with those reported for the [8.8.4] tiling structure.[3] The morphology is similar to a previously observed [8.8.4] tiling for BSV (0.9:1:1), where B represents poly(1,2-butadiene),[17] and for ISD (1:0.8:0.9) star, where D represents poly(dimethylsiloxane).[54] Increasing the V fraction further leads to a [12.6.4] tiling in the SCFT calculations as shown in Figures 1 and 2. It should be noted that this is an SCFT prediction only and if a sample with volume ratio ISV (1:1:1.6) is prepared under identical conditions as the other samples, then a [12.6.4] tiling would be the most plausible morphology.

Further increase in the length of V (ISV-1.9, ISV-2.9 and ISV-4.0) leads to CYLULAM morphology. The closest theoretical structure reported in literature is referred as "knitting pattern" in Ref. 2. Selective staining of the V domains with I_2 was used to identify whether V lamellae contain inclusions of either I of S. Judging from the uniformity of the V domains, neither I nor S was present in the V phase (SI3, Supporting Information). The bright protrusions (S) extending into the black phase in OsO_4 stained samples show that I forms discontinuous disk-like structure in the lamellae excluding V. To verify this, double staining with OsO_4 and I_2 was performed which provided sufficient contrast between all three components (Fig. 1). Double stained samples show that S forms a rather continuous phase along the V phase, resulting in an effective shielding of the black I domains from V. The CYLULAM structure can be described as a modified version of the LAM-3 structure, where the interface between V and S undulates, as opposed to being planar, and the lamellar structure of I surrounded by S is broken at regular intervals and filled by S. This leads to two different length scales (as shown in Fig. 1): the distance between two consecutive V or S lamellar domains (primary length scale) and the periodicity of the undulations, equivalent to the distance between the consecutive ellipse like domains of I within a lamella (secondary length scale). In the SCFT-based scattering patterns (Fig. 4), the peaks are assigned based on the oblique lattice formulation[55] (details are presented in SI4, Supporting Information). The first-order scattering peaks [10, 01, 11] are observed for all three ISV-1.9, ISV-2.9, and ISV-4 cases. Higher order scattering peaks [20, 30, 40] corresponding to the primary length scale [10] are observed up to third order for ISV-1.9, ISV-4 and up to fourth order for ISV-2.9. As the electron density difference between S and I is smaller compared to V and I, only one higher order peak [02] is observed for the secondary length scale in the case of ISV-1.9. In SAXS, qualitatively similar features are found up to the fifth order (Fig. 3) for the primary length scale, while only first-order peak is detected in the form of faint shoulders for the secondary length scale [Fig. 3(B)]. Observation of a very small and broad peak for the secondary length scale, [01] and/or [11], and the absence of higher order peak for this length scale may be attributed to PDI of the undulations and/or I domains. Moreover, the electron density difference between I and S is small in comparison to V and I. Similar detailed analysis of hierarchical lamellar microstructures in ABC star copolymers have been reported in Ref. 56.

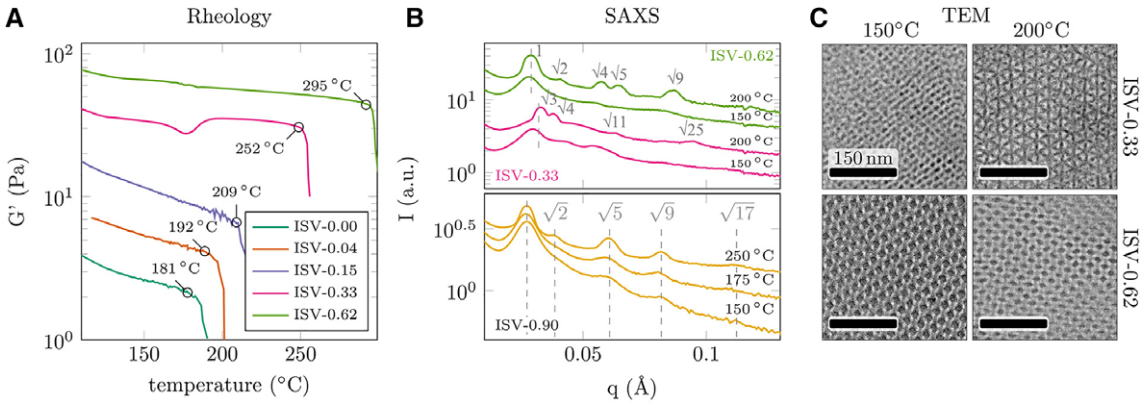

FIGURE 5 (A) Isochronal temperature scans data (ω = 1 rad s^{-1}, γ = 1%, 2 °C min^{-1}) for ISV-*x* samples with T_{ODT} < 300 °C. (B) Selected SAXS data for the samples ISV-0.33, ISV-0.62, and ISV-0.9 which were annealed at various temperatures. (C) Selected TEM images for the samples of ISV-0.33 and ISV-0.62 which were annealed at different temperatures. Typical absolute values of G' and G'' are provided in SI5, Supporting Information, for ISV-0.33. [Color figure can be viewed at wileyonlinelibrary.com]

Finally, increasing the length of V even further (ISV-5.2 and ISV-7.6) leads to hexagonally close packed structures, where the I domain is almost completely shielded from the V domain by S, which is attributed to the highest χ for I-V relative to the other two interacting pairs (see Table S1, Supporting Information). Both the TEM images and the SCFT-based morphology qualitatively agree with each other. Furthermore, the SAXS and the SCFT-based scattering patterns qualitatively agree with each other and they correspond to the hexagonally close packed structures with the peaks appearing in the ratio, 1:$\sqrt{3}$:$\sqrt{4}$.[5]

There are additional peaks near the primary peaks in the SCFT-based scattering patterns (ISV-0.33, ISV-0.43, ISV-5.2, and ISV-7.6 in Fig. 4), which result from hierarchical nature of the morphologies and the fact that these are three component systems. For the case of ISV-0.43, there are additional higher order peaks representing hierarchical nature of the morphology. Specifically, these additional peaks highlight that such morphologies are characterized by two length scales instead of one. We should point out that in Refs. 3,5, these additional peaks were incorrectly attributed to incommensurability between the simulation box sizes and period of the morphologies.

The morphologies of the ISV-*x* were compared to those reported in the literature (Table 2). The morphology reported for ISV-0.33 qualitatively agrees with previous reports based on the SCFT simulations, but the other morphologies (ISV-0.62, ISV-1.9, and ISV-2.9) do not agree. These differences may arise from differences in annealing temperatures, total molecular weights, and/or the microstructure of poly(isoprene): 1,4 or 3,4 addition, *cis* or *trans* conformation. We discuss each below.

Effects of Temperature

The complex shear modulus obtained during a temperature sweep (constant ramp rate of 2 °C min^{-1}) at fixed frequency and strain allows us to observe morphological transitions. The transitions are exemplified by a sudden change in the real part of the elastic modulus G' in Figure 5(A). In the simplest case of symmetric IS diblock copolymer, the evolution of G' as a function of temperature is continuous up to 181 °C and then a discontinuity is observed. This sudden decline of G' is associated with the ODT at T_{ODT}. Above T_{ODT}, the IS diblock copolymer transitions to a phase mixed state. For a symmetric AB diblock copolymer, T_{ODT} can be defined through a relation based on the mean field theory, written as $(\chi_{AB}N)_{ODT}$ = 10.5, where N is the total number of statistical segments of the diblock copolymer, and χ_{AB} is the Flory–Huggins interaction parameter characterizing interactions between A and B. T_{ODT} for symmetric IS was reported to be 100 °C and below 40 °C at molecular weights of 15 and 12 kDa, respectively.[57] Therefore, T_{ODT} = 181 °C, for the copolymer studied here with a molecular weight of 21.7 kDa is reasonable. By adding an extra V arm to the IS diblock copolymer, segmental mixing of all three I, S, and V components takes place at elevated temperature. The T_{ODT} for ISV-*x* stars with low V content (x = 0.04–0.62) exhibits a systematic shift to progressively higher values as the molecular weight of V increases [Fig. 5(A)].

One trend which is distinctive from others in Figure 5(A) is the abrupt increase of G' at 175 °C for ISV-0.33. Such behavior is attributed to the formation of another type of microstructure with a higher elastic modulus, despite the elevated temperature. For diblock copolymers, this behavior is normally explained by an order–order transition when crossing the boundaries in the morphology diagram (χN vs. volume fraction, f) as χ decreases with an increase in T (as $\chi \sim 1/T$).[37,49] The SAXS and TEM results are consistent with the rheology measurements. As shown in Figure 5(B) (SAXS results), the domain spacing of the sample ISV-0.33 decreases from 21.2 to 19.1 nm with an increase in temperature. This, along with change in the structure factor, as seen from relative peak positions, indicates that the phase transition must have occurred at elevated temperature resulting in a structure with smaller equilibrium domain spacing. The ISV-0.33 which was thermally annealed at 150 °C is characterized by a weak degree of order and adopts what appears to be a [12.6.4] and/or [8.6.6;

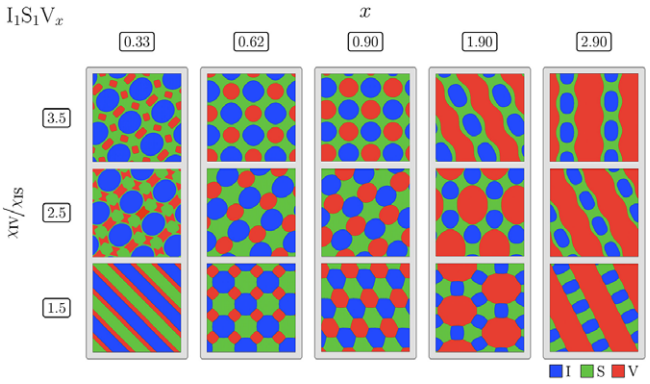

FIGURE 6 SCFT studies on the effect of χ_{IV}/χ_{IS} on the morphology of five different samples of ISV-*x* for qualitatively simulating the morphological changes. The morphology for ISV-0.33 changed from [12.6.4] tiling structure to LAM-3 as χ_{IV}/χ_{IS} is reduced from 3.5/2.5 to 1.5 the morphology for ISV-0.62 changed from [8.8.4] tiling to [6.6.6] tiling to [8.8.4] tiling as χ_{IV}/χ_{IS} is changed from 3.5 to 2.5 to 1.5. The morphology for ISV-0.9 changed from [8.8.4] tiling to [6.6.6] tiling as χ_{IV}/χ_{IS} is reduced from 3.5/2.5 to 1.5, both ISV-1.9 and ISV-2.9 formed CYLULAM structure at χ_{IV}/χ_{IS} = 3.5 but with reduction of χ_{IV}/χ_{IS} to 2.5/1.5 ISV-1.9 formed [12.6.4] tiling structure, whereas ISV-2.9 retained its CYLULAM structure for χ_{IV}/χ_{IS} = 2.5 and transformed to ALT.LAM when χ_{IV}/χ_{IS} was further lowered to 1.5. For all the cases, the dominating volume fraction of the component (I or S or V) was used to represent that particular grid point except for ISV-0.33. For ISV-0.33, the dominant I or S or if the volume fraction of V is greater than a cut-off value (from top to bottom the cut-off values are: 0.25, 0.22, and 0.2031) was used to represent the grid point. Color code: blue I, green S, red V. (See section SI6, Supporting Information for detailed equilibrium volume fraction profiles of all three components.) [Color figure can be viewed at wileyonlinelibrary.com]

8.6.4] morphology [Fig. 5(C)], while at 200 °C, a drastically different morphology was formed with relative peak positions of $\sqrt{3}$:$\sqrt{4}$:$\sqrt{11}$:$\sqrt{25}$ [Fig. 5(B)]. The microstructure is identified as a gyroid (GYR), since "wagon wheel" projections are clearly visible in the TEM micrograph [Fig. 5(C)]. In such scenario, gyroidal nets are formed by the I arm while S components are mixed with V, which is also in agreement with the scattering data. No shift in the first-order peak was observed for ISV-0.62 at 150 and 200 °C [Fig. 5(B)] indicating that the morphology remains unchanged up to T_{ODT} which is in agreement with rheology and TEM. Similarly, the sample ISV-0.9 shows stability and the absence of morphological transitions over a broad temperature range 150–250 °C [Fig. 5(B)]. The identical trend was observed for all ISV-*x* (*x* = 0.9–7.6) stars in rheology data (SI5, Supporting Information). Samples with higher V content (*x* = 0.9–7.6) have T_{ODT} exceeding the degradation temperature of the individual blocks (>300 °C) in agreement with the increase of their total molecular weight and therefore no attempts were made to observe the T_{ODT} experimentally for ISV-*x*, *x* = 0.9–7.6.

In summary, except for ISV-0.33, all other polymers retain their morphology over a wide range of temperatures (up to T_{ODT}) implying that temperature alone cannot explain the discrepancies in the observed morphologies of the ISV-*x* polymer samples compared to those reported in the literature of similar composition. Since the temperature dependence of χ_{IV} is unknown, no SCFT simulations were attempted to understand the effect of temperature on the morphology.

Qualitative Effects of Chemical Microstructure of Poly(isoprene) via χ_{IV}/χ_{IS}

There are three different interaction parameters for the ISV-*x*: χ_{IS}, χ_{SV}, and χ_{IV}, out of which the first and the third parameters are expected to be affected if the configuration of I is changed from predominantly *cis* 1,4 (present study) to predominantly 3,4 (reported in the literature).[58,59] However, quantitative details of changes in the chi parameters are not known experimentally. In this work, we systematically varied the ratio χ_{IV}/χ_{IS} to study its effects on the morphologies. It has been reported[3,26] that $\chi_{IS} \approx \chi_{SV} < \chi_{IV}$ for the morphologies investigated by Matsushita and coworkers.[4,24] In the present study, the effect of χ_{IV} was investigated while keeping the other two parameters fixed. The $\chi_{IV} = 3.5\times\chi_{IS}$, ($\chi_{IS}$ = 0.0737 at 175 °C) reported in the "Experimental" section was reduced by systematically decreasing the ratio χ_{IV}/χ_{IS} below 3.5. The ratio of 3.5 was obtained by scanning the parameter space to obtain the morphologies observed using TEM and SAXS in this work. The ratio was reduced to 2.5 and 1.5 to investigate the effect of χ_{IV} on the morphologies (Fig. 6). For ISV-0.33, decrease in χ_{IV}/χ_{IS} from 3.5/2.5 to 1.5 leads to LAM-3 structure from [12.6.4] tiling structure. For ISV-0.62, reduction in χ_{IV}/χ_{IS} from 3.5 to 2.5 to 1.5 leads to [8.8.4] to [6.6.6] to [8.8.4] tiling structure. ISV-0.9 undergoes transformation from [8.8.4] tiling to [6.6.6] tiling structure as χ_{IV}/χ_{IS} is reduced from 3.5/2.5 to 1.5. The ISV-1.9 transitioned from a CYLULAM structure to a [12.6.4] tiling morphology, as χ_{IV}/χ_{IS} was reduced from 3.5 to 2.5/1.5. Finally, ISV-2.9 retained a CYLULAM structure when χ_{IV}/χ_{IS} was reduced from 3.5 to 2.5 but it transformed into ALT. LAM structure with further reduction of χ_{IV}/χ_{IS} to 1.5, as expected for a more symmetric interaction case ($\chi_{IS} \approx \chi_{SV} \approx \chi_{IV}$).[3,33]

By systematically reducing the ratio χ_{IV}/χ_{IS} in the SCFT, we found that morphologies of ISV-*x* containing predominantly poly(3,4-isoprene) reported in the literature can be reproduced by decreasing χ_{IV}/χ_{SI} from 3.5 [ISV-*x* containing predominantly poly(*cis* 1,4-isoprene) to 2.5/1.5 for all of the four cases presented in Table 2 (ISV-0.33 forms [12.6.4] tiling at 2.5, ISV-0.62 forms [6.6.6] tiling at 2.5, ISV-1.9 forms [12.6.4] tiling both at 2.5 and 1.5, ISV-2.9 forms ALT.LAM at 1.5). With these calculations we demonstrated that the SCFT model can be used to qualitatively model the effects of microstructure of poly(isoprene) over a wide range of *x* values reported here.

In a previous report,[3] constant values of the interaction parameter were used for the different compositions of ISV-*x* where $N\chi_{IS} = N\chi_{SV}$ = 25.0 and χ_{IV}/χ_{IS} = 1.48. With these choices of parameters, the authors found the [8.8.4] structure to be more stable for ISV-0.7, rather than the reported [6.6.6]

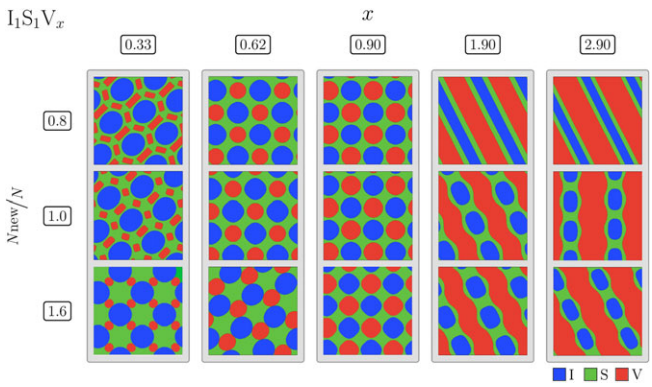

FIGURE 7 SCFT studies on the effects of simultaneously changing the three Flory–Huggins chi parameters via the ratio N_{new}/N. for the five different samples of ISV-*x*. ISV-0.33 transformed from [12.6.4] tiling to [8.8.4] tiling and ISV-0.62 changed from [8.8.4] tiling to [6.6.6] tiling as N_{new}/N was increased from 0.8 to 1.6. ISV-0.90 retained its [8.8.4] tiling structure for all the N_{new}/N values. ISV-1.9 and ISV-2.9 transformed from CYLULAM structure to LAM-3 structure as N_{new}/N was reduced from 1.6 to 0.8. For all the cases, the dominating volume fraction of the component (I or S or V) was used to represent that particular grid point except for ISV-0.33 (N_{new}/N = 0.8 and 1). For these two samples of ISV-0.33, the dominant I or S or if the volume fraction of V was greater than some cut-off value (0.25 for both N_{new}/N = 0.8 and 1) was used to represent a grid point. Color code: blue: I, green: S, red: V. These simulations highlight that not only the relative difference between the interaction parameters are important but also their absolute values. (See section SI7, Supporting Information for detailed equilibrium volume fraction profiles of all three components.) [Color figure can be viewed at wileyonlinelibrary.com]

tiling structure in the experiments.[18,19] However, their results agreed with the [8.8.4] and [12.6.4] for the case of ISV-1.2 and ISV-1.9, respectively.[18,19] Similarly, Jiang et al.[26] chose constant parameters for all the compositions of ISV-*x*, $N\chi_{IS} = N\chi_{SV} = 30.0$ and $\chi_{IV}/\chi_{IS} = 1.67$ in their SCFT calculations. With these parameters, they were able to qualitatively reproduce the morphologies reported in experiments[18] for $0.7 < x < 2.0$ but their results did not agree with the experimental results[4] for *x* values outside this range, which was attributed to smaller values of χN parameters. In experiments,[5,17,18] two arms are generally kept fixed and the third arm length is varied to tune the composition. This causes a change in the total molecular weight, and the assumption of a constant *N* can lead to discrepancies. In the following section, we explore these effects resulting from changes in the total molecular weights in an effort to reconcile differences with the reported results.

Effect of N

One of the factors that might have impact on the morphology of ISV-*x* star polymers is the total molecular weight for a given composition of I:S:V. For diblock copolymers $\chi N \sim N/T$, hence the temperature and molecular weight can be used interchangeably in defining the SCFT input parameter, χN. Whereas for terpolymers there are three different pairwise interactions, χ_{ij} (which are inversely proportional to the temperature *T*, with different proportionality constants for different pairs *i* and *j*) and just one *N*, therefore temperature dependence of the morphology diagrams is much more complicated for terpolymers than diblock copolymers. For most samples, the experimental morphologies were found to be independent of temperature, as reported in the earlier section. Since the temperature dependence of one of the pairs (χ_{IV}) is unknown, SCFT could not be undertaken to study the morphology as a function of temperature. The morphology of those samples may or may not be independent of molecular weight, which needs to be determined using SCFT. SCFT calculations were performed on five different samples of ISV-*x* to determine whether there is any transformation in the morphology due to a change in the *N* (leading to changes in $N\chi_{IS}$, $N\chi_{SV}$, and $N\chi_{IV}$). As shown in Figure 7, four of the five samples show transformations in morphology with the tuning of N_{new}/N, where N_{new} and *N* are the estimated and initial number of statistical segments for the samples, respectively (values tabulated in SI8, Supporting Information). ISV-0.33 transformed from [12.6.4] tiling morphology to [8.8.4] tiling when N_{new}/N was increased from 0.8/1 to 1.6. It should be noted that for ISV-0.33, V became miscible in S for N_{new}/N = 0.8 or 1 but it segregated when N_{new}/N was increased to 1.6. ISV-0.62 transformed from [8.8.4] tiling structure for N_{new}/N = 0.8 to [6.6.6] tiling structure for N_{new}/N = 1.6. ISV-0.90 retained its [8.8.4] tiling structure for all the N_{new}/N values. ISV-1.9 and ISV-2.9 behaved in a qualitatively similar manner, with a transformation from a CYLULAM structure to a LAM-3 structure as N_{new}/N was reduced from 1.6 to 0.8. Jiang et al.[26] observed LAM-3 structure instead of experimental results of ALT. LAM[4] reported for ISV-3 and they attributed their observation to smaller values of χN used in their calculations. Our results are in qualitative agreement with their speculation. This highlights that not only is the relative difference between the interaction parameters important, as reported by the SCFT studies[3,26] but also the absolute values of the interaction parameters as speculated previously.[26]

CONCLUSIONS

Miktoarm stars based on poly(*cis* 1,4-isoprene) (I), poly(styrene) (S), and poly(2-vinylpyridine) (V), allowed for systematic studies of the effects of composition, chemical microstructure, and temperature on the thermodynamics of microphase separation. For such studies, we have synthesized 11 ISV-*x* (I:S:V = 1:1:*x*, *v*:*v*:*v*) miktoarm stars. The morphologies of ISV-*x* consisting of predominantly poly(*cis* 1,4-isoprene) were determined using SAXS and TEM. The SCFT was used to model the systems over the entire composition range. These studies revealed a transition from a lamellar phase (ISV-0.04 and ISV-0.15) to different tiling phases ([12.6.4] and/or [8.6.6; 8.6.4]) for ISV-0.33, [8.8.4] for ISV-0.62 and ISV-0.9, CYLULAM structure for ISV-1.9, ISV-2.9 and ISV-4, and core–shell cylindrical morphology for ISV-5.2 and ISV-7.6. Some of these morphologies were different from those reported for similar compositions of ISV-*x* in the literature. These

differences were attributed to the chemical microstructure of the poly(isoprene) so that poly(*cis* 1,4-isoprene) and poly(2-vinylpyridine) are argued to microphase separate stronger compared to poly(3,4-isoprene) and poly(2-vinylpyridine). Also, the differences in molecular weights of our ISV systems were shown to influence the morphologies. As molecular weight increased, ISV-0.33 transformed from [12.6.4] tiling to [8.8.4], ISV-0.62 changed from [8.8.4] to [6.6.6] tiling morphology; ISV-1.9 and ISV-2.9 transformed from CYLULAM structure to LAM-3 structure as molecular weight decreased. The effect of temperature on the morphology was observed for ISV-0.33 which exhibited order–order transition to a gyroid phase at an elevated temperature. Our concerted effort on investigating the morphologies of ISV-*x* miktoarms using experimental and theoretical tools enhances the understanding of ISV-*x* structural properties in particular and ABC miktoarm polymers in general. This study highlights the importance of chemistry and molecular weight on the bulk morphologies of ISV-*x*, which can be probed in other polymeric systems for advancing our knowledge in ABC miktoarm copolymers.

ACKNOWLEDGMENTS

S Chernyy, J J K Kirkensgaard, K Mortensen, and K Almdal are thankful to Villum Foundation for the financial support of the project. Support by the Danish National Research Foundation, Project DNRF103 to K Almdal and L Schulte is acknowledged. Portions of the work including the computations were conducted at the Center for Nanophase Materials Sciences, which is a U.S. Department of Energy Office of Science User Facility. The Research at Oak Ridge National Laboratory's Spallation Neutron Source was sponsored by the Scientific User Facilities Division, Office of Basic Energy Sciences, U.S. Department of Energy (DOE). T P Russell and H Kim were supported by the Air Force Office of Scientific Research under contract 16RT1602. J P Mahalik and M M L Arras were supported by the Laboratory Directed Research and Development, Technology Innovation Program of ORNL managed by UT-Battelle, LLC for the U.S. Department of Energy.

REFERENCES

1 J. J. K. Kirkensgaard, M. C. Pedersen, S. T. Hyde, *Soft Matter* **2014**, *10*(37), 7182.

2 P. Tang, F. Qiu, H. Zhang, Y. Yang, *J. Phys. Chem. B* **2004**, *108*(24), 8434.

3 G. Zhang, F. Qiu, H. Zhang, Y. Yang, A.-C. Shi, *Macromolecules* **2010**, *43*(6), 2981.

4 Y. Matsushita, K. Hayashida, T. Dotera, A. Takano, *J. Phys. Condens. Matter* **2011**, *23*(28), 284111.

5 S. Chernyy, J. J. K. Kirkensgaard, J. P. Mahalik, H. Kim, M. M. L. Arras, R. Kumar, B. G. Sumpter, G. S. Smith, K. Mortensen, T. P. Russell, K. Almdal, *Macromolecules* **2018**, *55*(3), 1041.

6 M. Liu, W. Lia, F. Qiu, *J. Chem. Phys.* **2013**, *138*(10), 104904.

7 H. Deng, W. Li, F. Qiu, A.-C. Shi, *J. Phys. Chem. B* **2017**, *121*(17), 4642.

8 H. Hasegawa, Block Copolymers and Miktoarm Star-Branched Polymers. In *Springer Japan*, Anionic Polymerization, N. Hadjichristidis, A. Hirao Eds., **2015**, p. 843.

9 Y. Matsushita, A. Takano, K. Hayashida, T. Asari, A. Noro, *Polymer* **2009**, *50*(10), 2191.

10 J. J. K. Kirkensgaard, *Interface Focus* **2012**, *2*(5), 602.

11 J. J. K. Kirkensgaard, M. E. Evans, L. de Campo, S. T. Hyde, *Proc. Natl. Acad. Sci. U. S. A.* **2014**, *111*(4), 1271.

12 H. Iatrou, N. Hadjichristidis, *Macromolecules* **1992**, *25*(18), 4649.

13 S. Sioula, Y. Tselikas, N. Hadjichristidis, *Macromolecules* **1997**, *30*(5), 1518.

14 V. Bellas, H. Iatrou, N. Hadjichristidis, *Macromolecules* **2000**, *33*(19), 6993.

15 N. Hadjichristidis, S. Pispas, G. Floudas, Nonlinear Block Copolymers. In *Block Copolymers*, New Jersey: John Wiley & Sons, **2003**, p. 126.

16 H. Hückstädt, V. Abetz, R. Stadler, *Macromol. Rapid Commun.* **1996**, *17*(8), 599.

17 H. Hückstädt, A. Göpfert, V. Abetz, *Macromol. Chem. Phys.* **2000**, *201*(3), 296.

18 K. Hayashida, A. Takano, S. Arai, Y. Shinohara, Y. Amemiya, Y. Matsushita, *Macromolecules* **2006**, *39*(26), 9402.

19 A. Takano, S. Wada, S. Sato, T. Araki, K. Hirahara, T. Kazama, S. Kawahara, Y. Isono, A. Ohno, N. Tanaka, Y. Matsushita, *Macromolecules* **2004**, *37*(26), 9941.

20 R. Quirk, T. Yoo, *Polym. Bull.* **1993**, *31*(1), 29.

21 K. Hayashida, T. Dotera, A. Takano, Y. Matsushita, *Phys. Rev. Lett.* **2007**, *98*(19), 195502.

22 K. Hayashida, N. Saito, S. Arai, A. Takano, N. Tanaka, Y. Matsushita, *Macromolecules* **2007**, *40*(10), 3695.

23 K. Hayashida, W. Kawashima, A. Takano, Y. Shinohara, Y. Amemiya, Y. Nozue, Y. Matsushita, *Macromolecules* **2006**, *39*(14), 4869.

24 Y. Matsushita, *Macromolecules* **2007**, *40*(4), 771.

25 Y. Matsushita, K. Hayashida, A. Takano, *Macromol. Rapid Commun.* **2010**, *31*(18), 1579.

26 K. Jiang, J. Zhang, Q. Liang, *J. Phys. Chem. B* **2015**, *119*(45), 14551.

27 T. Gemma, A. Hatano, T. Dotera, *Macromolecules* **2002**, *35*(8), 3225.

28 C.-I. Huang, H.-K. Fang, C.-H. Lin, *Phys. Rev. E* **2008**, *77*(3), 031804.

29 J. J. K. Kirkensgaard, *Phys. Rev. E* **2012**, *85*(3), 031802.

30 W. Xu, K. Jiang, P. Zhang, A.-C. Shi, *J. Phys. Chem. B* **2013**, *117*(17), 5296.

31 A. Arora, J. Qin, D. C. Morse, K. T. Delaney, G. H. Fredrickson, F. S. Bates, K. D. Dorfman, *Macromolecules* **2016**, *49*(13), 4675.

32 F. S. Bates, M. A. Hillmyer, T. P. Lodge, C. M. Bates, K. T. Delaney, G. H. Fredrickson, *Science* **2012**, *336*(6080), 434.

33 W. Li, Y. Xu, G. Zhang, F. Qiu, Y. Yang, A.-C. Shi, *J. Chem. Phys.* **2010**, *133*(6), 064904.

34 A. Nunns, C. A. Ross, I. Manners, *Macromolecules* **2013**, *46*(7), 2628.

35 R. E. Cohen, D. Wilfong, *Macromolecules* **1982**, *15*(2), 370.

36 S. Ndoni, C. M. Papadakis, F. S. Bates, K. Almdal, *Rev. Sci. Instrum.* **1995**, *66*(2), 1090.

37 M. F. Schulz, A. K. Khandpur, F. S. Bates, K. Almdal, K. Mortensen, D. A. Hajduk, S. M. Gruner, *Macromolecules* **1996**, *29*(8), 2857.

38 S. Chernyy, J. J. K. Kirkensgaard, A. Bakke, K. Mortensen, K. Almdal, *Polymer* **2017**, *133*, 129.

39 S. Chernyy, Z. Wang, J. J. K. Kirkensgaard, A. Bakke, K. Mortensen, S. Ndoni, K. Almdal, *J. Polym. Sci. Part A: Polym. Chem.* **2017**, *55*(3), 495.

40 G. M. Grason, R. D. Kamien, *Phys. Rev. E* **2005**, *71*(5), 051801.

41 G. M. Grason, *Phys. Rep.* **2006**, *433*(1), 1.

42 G. Fredrickson, *The Equilibrium Theory of Inhomogeneous Polymers*, Oxford University Press, New York, **2006**; Vol. *134*.

43 G. Tzeremes, K. Ø. Rasmussen, T. Lookman, A. Saxena, *Phys. Rev. E* **2002**, *65*(4), 041806.

44 S. W. Sides, G. H. Fredrickson, *Polymer* **2003**, *44*(19), 5859.

45 https://www.txcorp.com

46 R. Kumar, S. W. Sides, M. Goswami, B. G. Sumpter, K. Hong, X. Wu, T. P. Russell, S. P. Gido, K. Misichronis, S. Rangou, A. Avgeropoulos, T. Tsoukatos, N. Hadjichristidis, F. L. Beyer, J. W. Mays, *Langmuir* **2013**, *29*(6), 1995.

47 K. Misichronis, J. Chen, A. Imel, R. Kumar, J. Thostenson, K. Hong, M. Dadmun, B. G. Sumpter, J. G. Kennemur, N. Hadjichristidis, J. W. Mays, A. Avgeropoulos, *Macromolecules* **2017**, *50*(6), 2354.

48 M. W. Schulze, R. M. Lewis, J. H. Lettow, R. J. Hickey, T. M. Gillard, M. A. Hillmyer, F. S. Bates, *Phys. Rev. Lett.* **2017**, *118*(20), 207801.

49 A. K. Khandpur, S. Foerster, F. S. Bates, I. W. Hamley, A. J. Ryan, W. Bras, K. Almdal, K. Mortensen, *Macromolecules* **1995**, *28*(26), 8796.

50 W. Zha, C. D. Han, D. H. Lee, S. H. Han, J. K. Kim, J. H. Kang, C. Park, *Macromolecules* **2007**, *40*(6), 2109.

51 Y. Funaki, K. Kumano, T. Nakao, H. Jinnai, H. Yoshida, K. Kimishima, K. Tsutsumi, Y. Hirokawa, T. Hashimoto, *Polymer* **1999**, *40*(25), 7147.

52 Frigo, M. In Proceedings of the 1999 ACM SIGPLAN Conference on Programming Language Design and Implementation (PLDI '99), 1999; ACM: Atlanta, GA, USA, **1999**; pp 169–180.

53 R. Kumar, B. S. Lokitz, S. W. Sides, J. Chen, W. T. Heller, J. F. Ankner, J. F. Browning, S. M. Kilbey Ii, B. G. Sumpter, *RSC Adv.* **2015**, *5*(27), 21336.

54 K. Yamauchi, K. Takahashi, H. Hasegawa, H. Iatrou, N. Hadjichristidis, T. Kaneko, Y. Nishikawa, H. Jinnai, T. Matsui, H. Nishioka, M. Shimizu, H. Furukawa, *Macromolecules* **2003**, *36*(19), 6962.

55 D. Marsh, *Chem. Phys. Lipids* **2012**, *165*(1), 59.

56 X. Yuci, L. Weihua, Q. Feng, Z. Hongdong, Y. Yuliang, S. An-Chang, *J. Polym. Sci. B* **2010**, *48*(10), 1101.

57 N. Sakamoto, T. Hashimoto, *Macromolecules* **1995**, *28*(20), 6825.

58 D. J. Worsfold, S. Bywater, *Can. J. Chem.* **1964**, *42*(12), 2884.

59 F. S. Bates, J. H. Rosedale, H. E. Bair, T. P. Russell, *Macromolecules* **1989**, *22*(6), 2557.